Nanoscale Advances

PAPER

View Article Online
View Journal | View Issue

Check for updates

Cite this: *Nanoscale Adv.*, 2022, **4**, 4658

The benefits of combining 1D and 3D nanofillers in a piezocomposite nanogenerator for biomechanical energy harvesting†

Zouhair Hanani, *[abc] Ilyasse Izanzar,[a] Soukaina Merselmiz,[a] M'barek Amjoud,[a] Daoud Mezzane,[ad] Jaafar Ghanbaja,[e] Ismael Saadoune,[af] Mohammed Lahcini,[af] Matjaž Spreitzer,[c] Damjan Vengust,[c] Mimoun El Marssi,[d] Zdravko Kutnjak,[c] Igor A. Luk'yanchuk[dg] and Mohamed Gouné[b]

Received 1st July 2022
Accepted 26th September 2022

DOI: 10.1039/d2na00429a

rsc.li/nanoscale-advances

Mechanical energy harvesting using piezoelectric nanogenerators (PNGs) offers an attractive solution for driving low-power portable devices and self-powered electronic systems. Here, we designed an eco-friendly and flexible piezocomposite nanogenerator (c-PNG) based on $H_2(Zr_{0.1}Ti_{0.9})_3O_7$ nanowires (HZTO-nw) and $Ba_{0.85}Ca_{0.15}Zr_{0.10}Ti_{0.90}O_3$ multipods (BCZT-mp) as fillers and polylactic acid (PLA) as a biodegradable polymer matrix. The effects of the applied stress amplitude, frequency and pressing duration on the electric outputs in the piezocomposite nanogenerator (c-PNG) device were investigated by simultaneous recording of the mechanical input and the electrical outputs. The fabricated c-PNG shows a maximum output voltage, current and volumetric power density of 11.5 V, 0.6 μA and 9.2 mW cm^{-3}, respectively, under cyclic finger imparting. A high-pressure sensitivity of 0.86 V kPa^{-1} (equivalent to 3.6 V N^{-1}) and fast response time of 45 ms were obtained in the dynamic pressure sensing. Besides this, the c-PNG demonstrates high-stability and durability of the electrical outputs for around three months, and can drive commercial electronics (charging capacitor, glowing light-emitting diodes and powering a calculator). Multi-physics simulations indicate that the presence of BCZT-mp is crucial in enhancing the piezoelectric response of the c-PNG. Accordingly, this work reveals that combining 1D and 3D fillers in a polymer composite-based PNG could be beneficial in improving the mechanical energy harvesting performances in flexible piezoelectric nanogenerators for application in electronic skin and wearable devices.

1. Introduction

Since 2006, the concept of piezoelectric energy harvesting, proposed by Wang *et al.*,[1] using a piezoelectric nanogenerator (PNGs) has become a growing and a promising technology for converting random mechanical energy into electric energy using nanoscale piezoelectric materials.[2–4] Another biomechanical energy harvesting concept is the use of triboelectric nanogenerators.[5–8] However, despite their high electrical outputs, the impermanent nature of triboelectric charges limits their long-term durability.[9] Besides this, contrary to chemical batteries, PNGs can provide sustainable electrical energy.[2] In particular, ceramic/polymer piezocomposites for energy harvesting applications are considered to be a significant research field, providing the convenience of mechanical flexibility, adaptability for large mechanical forces, suitable voltage with sufficient power output, lower internal leakage current, lower manufacturing costs, and rapid processing compared to ceramic-based PNGs.[2,10–12] In this case, both the ceramic and polymer must be carefully selected.[2] However, the most high-performance piezoceramics used in industry, such as $PbZr_xTi_{1-x}O_3$ (PZT), are lead-based, toxic and environmentally unfriendly, and thus their integration in future applications will be restricted.[13–17] Similarly, the majority of polymers used in polymer-based PNGs, such as polydimethylsiloxane (PDMS) and polyvinylidene fluoride (PVDF), are petrol-based, not eco-friendly and the majority of them are not biodegradable.[3,18–20] Besides this, almost all PNGs require a poling process to promote the piezoelectric activity of the utilised materials.[19,21–23] Consequently, the durability of the output performances of these PNGs have been questioned.[24–26] Recently, we designed

---

[a] IMED-Lab, Cadi Ayyad University, Marrakesh, 40000, Morocco. E-mail: zouhair.hanani@ijs.si

[b] ICMCB, University of Bordeaux, Pessac, 33600, France

[c] Jozef Stefan Institute, Ljubljana, 1000, Slovenia

[d] LPMC, University of Picardy Jules Verne, Amiens, 80039, France

[e] IJL, University of Lorraine, 54000, Nancy, France

[f] Mohammed VI Polytechnic University, Ben Guerir, 43150, Morocco

[g] Department of Building Materials, Kyiv National University of Construction and Architecture, Kyiv, Ukraine

† Electronic supplementary information (ESI) available. See DOI: https://doi.org/10.1039/d2na00429a

a self-poled and bio-flexible piezoelectric nanogenerator (BF-PNG) based on lead-free biocompatible $Ba_{0.85}Ca_{0.15}Zr_{0.10}Ti_{0.90}O_3$ (BCZT) nanoparticles that are functionalised with polydopamine and embedded in a polylactic acid (PLA) biodegradable polymer.[27] The BF-PNG was able to generate excellent electrical outputs under gentle finger tapping, and demonstrated outstanding mechanical robustness, stable and durable output even after one year.

It has been reported that 1D-shaped piezoelectric nanowires are better than 0D ones for energy harvesting applications.[28,29] To tailor piezocomposites with high electrical outputs, the design of novel piezo-fillers with complex morphologies unlike 0D-nanoparticles and 1D-nanomaterials (nanowires, nanotubes, nanofibers, *etc.*) is a leading topic. Previously, we reported the piezoelectric energy harvesting of lead-free $H_2(Zr_{0.1}Ti_{0.9})_3O_7$ nanowires embedded in a PLA matrix and observed enhanced output performances (open-circuit voltage of 5.41 V and short-circuit current of 0.26 μA) and could drive small commercial electronics under various human motions).[30]

To further improve the piezoelectric energy harvesting properties of nanogenerators, the design of other complex morphologies is attracting considerable critical attention. Mainly, the use of 3D fillers (*e.g.* flowers, stars, *etc.*) is gaining interest in the scientific community.[31–33] More specifically, flower-like piezo-fillers with a 3D morphology play a vital role in enhancing piezoelectric harvesting performances.[32] Accordingly, the combination of 1D and 3D piezoceramics could enhance further the piezoelectric response of piezoelectric nanogenerators.

From this perspective, we report a novel strategy to design ceramic/polymer nanocomposites for energy harvesting applications. This involves embedding $H_2(Zr_{0.1}Ti_{0.9})_3O_7$ nanowires (HZTO-nw) and $Ba_{0.85}Ca_{0.15}Zr_{0.10}Ti_{0.90}O_3$ multipods (BCZT-mp) in a PLA biopolymer. The effects of the applied stress amplitude, frequency and pressing duration on the electric outputs in the piezocomposite nanogenerator device (c-PNG) were investigated using a simultaneous recording of the mechanical input and the electrical outputs. Through this approach, enhanced output voltage and a short-circuit current of 11.5 V and 0.6 μA, respectively, were obtained under finger tapping. Multi-physics simulations using COMSOL Multiphysics indicated that the presence of the BCZT-mp was crucial in enhancing the piezoelectric response of the c-PNG. In addition, the c-PNG can generate stable and durable voltage even after three months. The c-PNG proved its applicability to generate enhanced output voltage under bending motions, and to drive low-power commercial electronics (light-emitting diodes (LEDs) and a calculator).

2. Experimental section

2.1. Preparation of HZTO-NWs

To produce $H_2(Zr_{0.1}Ti_{0.9})_3O_7$ nanowires (HZTO-nw),[34] which serve as an inorganic template for BCZT multipod preparation, 5 g of $Zr_{0.1}Ti_{0.9}O_2$ (ZTO) powder synthesised previously[35] was dispersed in 100 mL of a 10 M aqueous solution of NaOH. After 1 h of stirring, the suspension was transferred to a 150 mL Teflon-lined stainless-steel autoclave, sealed and heated at 240 °C for 48 h, then cooled to room temperature. The resulting white suspension was collected by filtration and soaked in 0.2 M HCl for 10 h to convert $Na_2(Zr_{0.1}Ti_{0.9})_3O_7$ (NaZTO) to $H_2(Zr_{0.1}Ti_{0.9})_3O_7$ (HZTO). The obtained product was centrifuged at 4000 rpm for 10 min, washed several times with deionised water and ethanol, filtered, then freeze-dried for 48 h to obtain a fluffy product. The detailed structural, morphological and piezoelectric characterisation can be found in the literature.[30,36]

2.2. Preparation of BCZT multipods

BCZT multipods were prepared *via* the hydrothermal reaction of HZTO-nw with barium acetate and calcium nitrate tetrahydrate, as reported in ref. 37. Under an inert atmosphere (N_2), 150 mg of HZTO-NWs was dispersed in 35 mL of barium acetate (50 mM) and calcium nitrate tetrahydrate (8.8 mM) solution and 0.1 M of potassium hydroxide. Next, the suspension was sonicated for 10 min to break the agglomeration. Then, the suspension was purged with N_2, transferred into a 50 mL-Teflon-lined stainless-steel autoclave, sealed and heated at 180 °C for 6 h. Once the hydrothermal reaction was completed, the sealed autoclave was cooled down to room temperature. The resulting white precipitate was collected by centrifugation at 5000 rpm for 10 min, soaked in 0.2 M HCl for 4 h, and washed several times with 0.2 M HCl, deionised water and ethanol. Then, the final product was dried at 80 °C for 12 h. Since the growth of BCZT-mp is based on HZTO-nw, which serves as a template, and the conversion is not complete, as discussed previously,[36] the final product contains both HZTO-nw and BCZT-mp in a ratio of 1 : 5.

2.3. Preparation of the HZTO-nw + BCZT-mp/PLA nanocomposite film

The resulting nanopowder was functionalised with polydopamine (PDA) to enhance the dispersion stability and to avoid agglomeration formation, as we reported previously in the literature.[27] HZTO-nw + BCZT-mp/PLA nanocomposite films were modified using the solution casting method employing 0, 5, 10, 20, 30 and 40 vol% of the inorganic filler, as illustrated in Fig. 1a. Explicitly, an adequate amount of PLA was solubilised in dichloromethane with magnetic stirring for 2 h. Subsequently, the HZTO-nw + BCZT-mp were dispersed therein using ultrasound for 15 min, then homogenised by magnetic stirring for another 2 h. The slurry was cast in a Teflon Petri dish, dried at room temperature to obtain a flexible composite film, dried under vacuum at 40 °C for 12 h to remove the solvent, then finally hot-pressed at 140 °C for 15 min to reduce porosity.

2.4. Fabrication of the c-PNG device

PLA-based piezocomposite films using 0, 5, 10, 20, 30 and 40 vol% HZTO-nw + BCZT-mp filler (c-PNG) were sandwiched between two copper foils of 1.7 × 1.4 cm^2 serving as top and bottom electrodes. For external connections, two copper wires were attached to the top and bottom electrodes to measure the electrical outputs. Then, the c-PNG was additionally sandwiched by using Kapton® tape. This encapsulation prevents

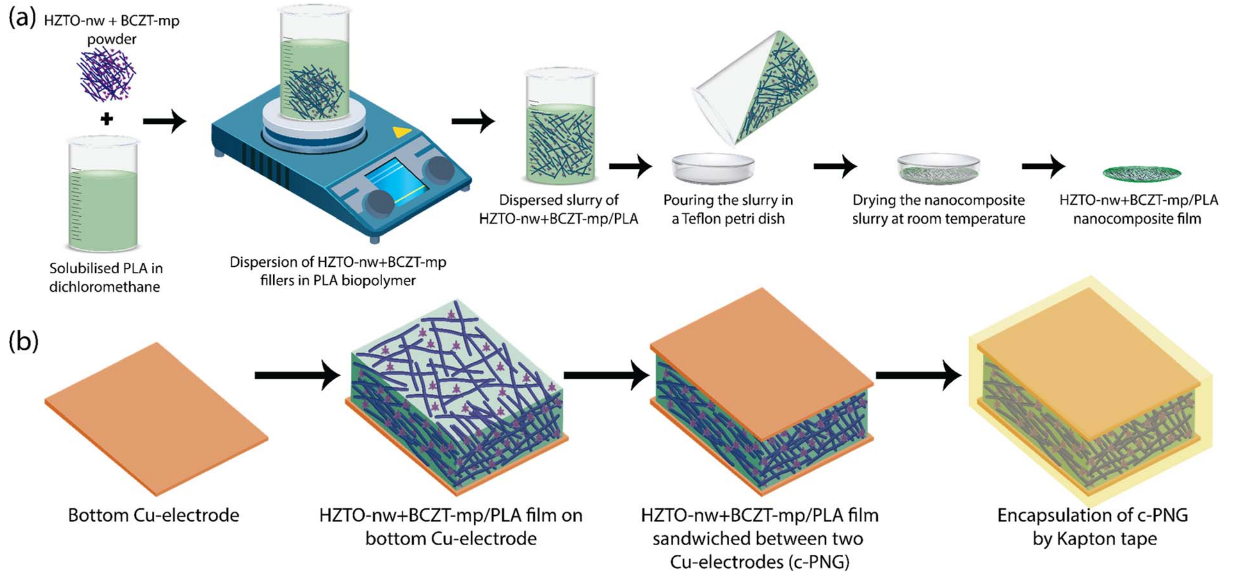

Fig. 1 Experimental procedure for the preparation of (a) the 20 vol% HZTO-nw + BCZT-mp/PLA nanocomposite film and (b) the c-PNG device.

damage of the c-PNG by repeated mechanical excitation and makes it water- and dustproof. Fig. 1b summarises the fabrication process of the c-PNG.

2.5. Characterisation

The morphological properties of the filler powder and the HZTO-nw + BCZT-mp/PLA nanocomposite film were analysed by using a scanning electron microscope equipped with an electron gun (FESEM, JEOL JSM-7600F). An energy-dispersive X-ray (EDX) spectrometer was utilised to confirm the composition of the BCZT multipods, and a backscattered electron detector (BSE) was used to visualise the cross-section of the nanocomposite film, including all its components (HZTO-nw, BCZT-mp and PLA). A transmission electron microscope (JEOL – ARM 200F Cold FEG TEM/STEM) operating at 200 kV coupled with a high-angle annular dark-field (HAADF) detector was used to visualise the morphology of the BCZT multipods. A Discovery Series TGA 55 (TA instruments) device was used to characterise the thermal stability of PLA and HZTO-nw + BCZT-mp/PLA during the heating process. About 8 mg of the sample was placed in a platinum pan and heated from room temperature to 600 °C at a heating rate of 10 °C min^{-1} under a nitrogen flow of 40 mL min^{-1}. The average thickness of the nanocomposite film was measured using a precise coating thickness gauge (Surfix Pro S, Phynix). To study the output performances of the piezocomposite nanogenerator (c-PNG), the open-circuit voltage, short-circuit current and electrical charge were measured using a potentiostat (SP-150, Bio-Logic). The approximate contact force of finger tapping was evaluated experimentally using a dual column mechanical testing system (Instron, 3369). The tensile mechanical behaviour of the films was performed using a crosshead speed of 5 mm min^{-1}. All measurements were carried out at room temperature.

3. Results and discussion

3.1. Structural and morphological properties

Fig. 2a shows the FESEM micrograph of the filler nanopowder composed mainly of 1D-HZTO nanowires (HZTO-nw) with a high aspect ratio, and 3D-BCZT multipods (BCZT-mp). Fig. 2b presents a STEM-HAADF image of a single BCZT multipod with a 500 nm pod-length six-pod architecture. The composition of the BCZT multipods was confirmed by energy dispersive X-ray (EDX) analyses, as shown in Fig. S1 and S2 (ESI).† The growth mechanism of the BCZT multipods has previously been thoroughly discussed.[36] The X-ray diffractometry (XRD) pattern of the nanopowder is illustrated in Fig. 2c, wherein the presence of BCZT-mp and HZTO-nw can be clearly observed, and HZTO-nw and BCZT-mp can be observed to have crystallised in monoclinic ($C2/m$) and tetragonal ($P4mm$) phases, respectively. As depicted in the inset of Fig. 2c, the selected area electron diffraction SAED pattern clearly shows that the BCZT multipod is single crystalline and has a good crystalline phase. As shown in the SAED pattern, the lattice spacings determined from the diffraction spots of the SAED of the BCZT multipod are 3.999 Å and 2.834 Å, which match the (100) and (011) planes, respectively. The corresponding zone axis (ZA) of the SAED pattern is indicated in the top of the figure. Further structural, morphology and composition analyses of the BCZT multipods can be found in the literature.[36] Besides this, Fig. 2d presents an FESEM image of the cross-section of the 20 vol% HZTO-nw + BCZT-mp/PLA nanocomposite film, from which a dense film with 8 μm thickness is observed (the cross-section of the nanocomposite with low magnification is provided in Fig. S3 (ESI)).† In the FESEM images, a BSE detector was used to visualise the composition fluctuation in the nanocomposite film, where the whitest spots represent the BCZT multipods. Also, it can be clearly seen that HZTO-nw and BCZT-mp fillers are

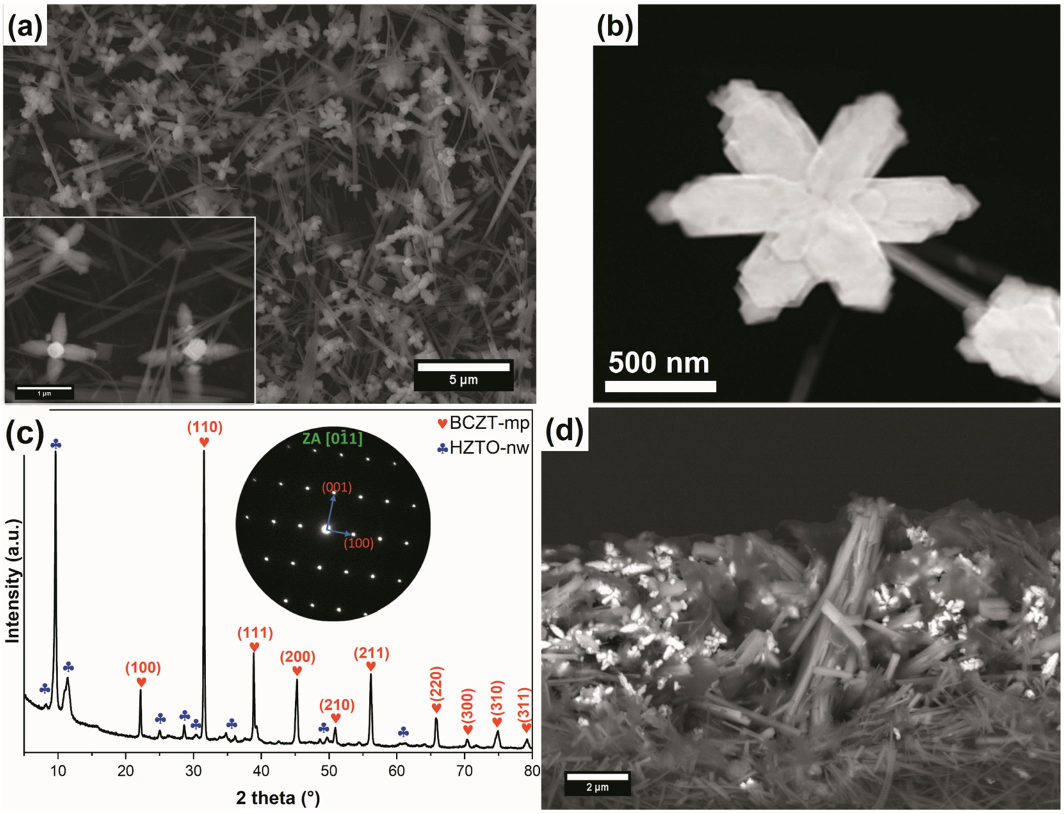

Fig. 2 (a) FESEM micrograph of the raw nanopowder (inset shows the magnified view of the BCZT multipods and HZTO nanowires). (b) STEM-HAADF image of a single BCZT multipod. (c) XRD pattern of the raw nanopowder (inset is the SAED pattern of a single BCZT multipod). (d) FESEM image of a cross-section of the 20 vol% HZTO-nw + BCZT-mp/PLA nanocomposite film.

covered with PLA polymer matrix, indicating the excellent compatibility between PLA and the fillers.[38,39]

The mechanical and thermal properties of PLA and 20 vol% HZTO-nw + BCZT-mp/PLA films are depicted in Fig. S4† (ESI).† Thermogravimetric analysis (TGA) was used to evaluate the effect of HZTO-nw + BCZT-mp fillers on the thermal stability of the PLA biopolymer. Fig. S4a† shows the TGA curves and their respective derivative thermogravimetry (DTG) curves (inset of Fig. S4a†) of the neat PLA and 20 vol% HZTO-nw + BCZT-mp/PLA films. Both TGA curves display one decomposition step between 240 and 350 °C. It is observed that PLA and 20 vol% HZTO-nw + BCZT-mp/PLA start to degrade from 240 and 250 °C, respectively, as defined from the onset degradation temperatures in the DTG curves. This improvement in the thermal behaviour (shift in the TGA curve of the nanocomposite film toward higher temperatures) is related to the presence of HZTO-nw + BCZT-mp as a reinforcing charge.[40,41] The mass residues at 600 °C are 0.63 and 7.79% for the PLA and 20 vol% HZTO-nw + BCZT-mp/PLA films, respectively.

Meanwhile, Fig. S4b† depicts the typical stress–strain curves of the neat PLA and 20 vol% HZTO-nw + BCZT-mp/PLA films. Obviously, both samples exhibit a clearly distinguished yield point, as shown in Fig. S4b.† After loading the PLA with HZTO-nw + BCZT-mp fillers, the Young's modulus (Y) doubled from 26.33 to 53.05 MPa. Accordingly, the 20 vol% HZTO-nw + BCZT-mp/PLA nanocomposite films can resist high mechanical stress and exhibit a relatively high Young's modulus.[42] Actually, good mechanical properties of the piezocomposite film are highly required to preserve the designed piezoelectric nanogenerator from damage while applying mechanical impartation during the energy harvesting process.[43,44]

3.2. Mechanical energy harvesting of the c-PNG

To assess the biomechanical energy harvesting ability of the modified piezocomposite films, piezoelectric nanogenerators with different filler concentrations (0, 5, 10, 20, 30 and 40 vol%) were designed. Fig. 3a shows a schematic illustration of the developed flexible piezocomposite nanogenerator device (c-PNG), consisting of a 20 vol% HZTO-nw + BCZT-mp/PLA nanocomposite film sandwiched between two copper electrodes and embedded with Kapton® tape, while Fig. 3b shows a photograph of the flexible piezocomposite nanogenerator device under bending motion, proving its flexibility. To gain insight on the effects of HZTO-nw + BCZT-mp filler concentration on the piezoelectric performance, specifically the open circuit voltage (V_{oc}), the fabricated nanogenerators were subjected to finger impartations of 2 N and the resulting V_{oc} values were recorded and are presented in Fig. S5 in the ESI.† It was observed that the output voltage was amplified with an increase in the HZTO-nw + BCZT-mp concentration. This can be explained by an enhancement in the dielectric constant of the

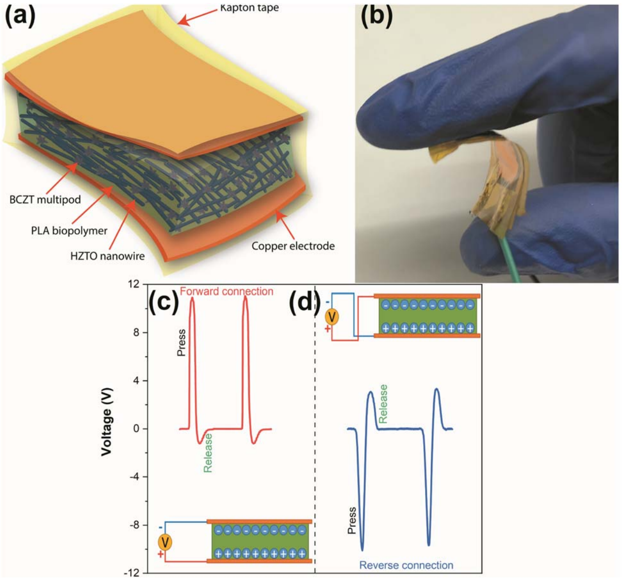

Fig. 3 (a) Illustration and (b) photograph of the fabricated piezocomposite nanogenerator. The generated open-circuit voltage when the external circuit is connected in the (c) forward and (d) reverse directions.

composite with filler addition, and nanocomposite films with a higher dielectric constant show good storage charge capability, which can lead to better piezoelectric properties.[45] Nevertheless, above 20 vol%, a decline in the piezoelectric performance is observed due to filler agglomeration, *i.e.* deterioration of the mechanical properties which limits the movement of PLA dipoles and eventually weakens the polarizability of the nanocomposite.[46] Subsequently, the focus will only be on a piezocomposite with 20 vol% HZTO-nw + BCZT-mp.

Interestingly, compared to other previously reported PNGs, our piezoelectric nanocomposite energy harvester does not require any poling process to promote its piezoelectric activity. To verify the purity of piezoelectric effects in the PNG device, a switching polarity test was conducted.[47] As presented in Fig. 3c, upward and downward output signals were obtained upon pressing and releasing motions, respectively, when the c-PNG device was forward-connected to the measurement kit. In contrast, the signal direction was inverted in the reverse connection, as shown in Fig. 3d. The observation of such signal output switching by changing the polarity confirms that the energy harvesting signals are the product of piezoelectricity from the flexible c-PNG device.[29,48]

A dual column mechanical testing system and an electrical measurement unit was employed to simultaneously record the input stress and output voltage. First, we examined the effect of applied stress on the electrical output performances, and the results are given in Fig. 5a and b. Real-time simultaneous recording of the open-circuit voltage and the stress amplitude under finger tapping is presented in Video S1 in the ESI.† It can be clearly seen that increasing the mechanical input (mechanical stress) enhances the electrical output (open-circuit voltage) of the c-PNG. For instance, by applying 2.97 kPa, an open-circuit voltage of 5.73 V can be obtained, however, by increasing the mechanical stress to 9.90 kPa, an open-circuit voltage of 11.04 V can be reached. The value discrepancy of each peak can be ascribed to the different strain rate of the device during the press-release process.[47] Besides this, the observed asymmetry in the positive and negative voltage peaks is attributed to the difference between the external force applied on the device and the restoring force.[49]

These results are consistent with the dependence of the crystal structure deformation on the applied mechanical stress. A simulation of the piezoelectric potential of the c-PNG device by finite element (FEA) method using the COMSOL Multiphysics 5.6 programming software under a mechanical stress of 2 N is depicted in Fig. 4. Simulation calculations of the piezopotential involved solid mechanics, the electrostatic effect, and the piezoelectric effect. By applying a mechanical stress of 2 N, positive and negative piezopotentials of 13 and −3 V were found. From Fig. 4a, it can be seen that the effective stress occupies a large area in the HZTO nanowires, however, highly

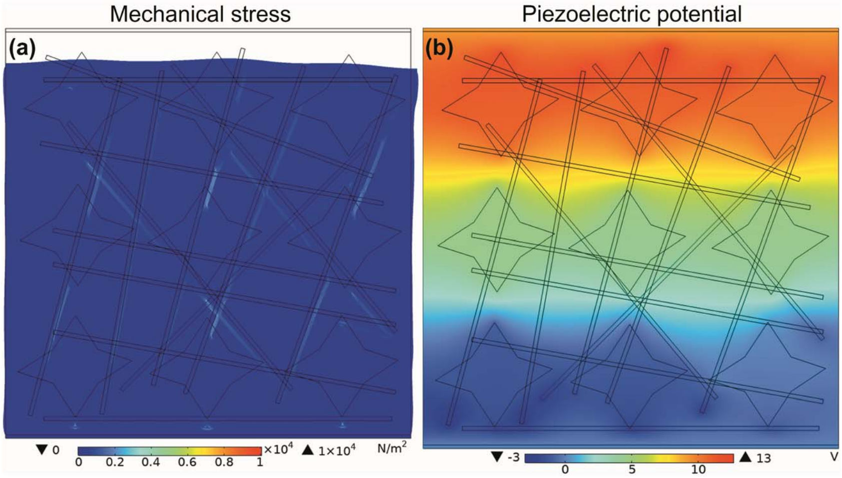

Fig. 4 The simulated distribution by FEA of (a) mechanical stress and (b) piezoelectric potential under a compression of 2 N.

effective stress is mainly applied to the corners of the BCZT multipods (brighter colour) compared to that applied to the centre. This can be explained by the extension of the applied stress to the corner of the BCZT-mp under external pressure to the composite. This stress distribution discontinuity is believed to be related to the specific space architecture of BCZT-mp, which was not observed in HZTO-nw. Similar observations were reported by Jian *et al.*[32] Therefore, the high local stress at BCZT-mp may be the main reason for the significantly enhanced voltage output in the c-PNG. A confirmation of these observations is presented in Fig. S6 (ESI),† where we simulated the mechanical stress and piezoelectric potential under a compression of 2 N of c-PNG using different fillers. It was found that the presence of BCZT-mp is vital in enhancing the piezoelectric response of the c-PNG.

The mechanical energy harvesting at various frequencies was studied using a constant stress of about 10.50 kPa (Fig. 5c and d). As observed, the generated output voltage is not impacted by increasing the operating frequency from 1 to 5 Hz, indicating that the c-PNG device has the potential to scavenge mechanical energy with adjustable frequency and amplitude in a natural environment.

Also, the effect of the pressing duration on the open-circuit voltage was investigated and the results are provided in Fig. 5e and f. A demonstration of the real-time simultaneous recording of the open-circuit voltage and the applied stress duration under finger tapping is depicted in Video S2 (ESI).† From first sight, it can be observed that using high mechanical stress does not result in a high output voltage. However, a thorough observation of the output voltage indicates that applying high mechanical stress results in symmetric voltage peaks. Besides this, contrary to the “press-release” sequence, the “press-hold-release” sequence produces output voltage peaks with greater negative voltage. This indicates that when applying low mechanical stress, the charges are hardly fully-pushed from one electrode to another.[50] It is worth mentioning that the stress drop in the hold sequence is related to the finger trembling while pressing (Fig. 5f). The peak-to-peak voltage ($\Delta V_{\text{p-p}}$) was found to increase with increasing stress amplitude and hold time. For instance, $\Delta V_{\text{p-p}}$ is enhanced from 13.4 to 17.8 V upon increasing the applied mechanical stress from 9.9 to 62.5 kPa, respectively. Notably, $\Delta V_{\text{p-p}}$ can be further improved by adding a hold sequence (pressing duration) in the input stress. For example, by applying only 45.4 kPa with a hold time of 3 s, the ΔV_{p-p} can be boosted to 23.2 V, compared to that obtained by applying 62.5 kPa.

The sensitive properties of the c-PNG at low pressures ($\Delta\sigma \leq$ 10 kPa) were evaluated through the dynamic pressure sensitivity (S) according to $S = \Delta V_{P-P}/\Delta\sigma$, where $\Delta V_{\text{p-p}}$ and $\Delta\sigma$ are the differences in the generated peak-to-peak voltage and applied stress, respectively.[51,52] From Fig. S7 (ESI),† the generated output voltage changes almost linearly with respect to the increased implied pressure. The calculated sensitivity of the c-PNG was found to be 0.86 V kPa^{-1}, equivalent to 3.61 V N^{-1}, which is higher than several previously reported piezoelectric pressure sensors.[52–61] Another important parameter in sensors is the sensing response time. By applying a pressure of 10.50 kPa, the c-PNG can delivers a fast response of 45 ms at 1 Hz. The response time of the c-PNG increases as the frequency of the applied pressure decreases, mainly due to a decrease of the applied pressure speed.[62] These response times are lower than those of other reported piezoelectric sensors.[52,63–66] These outcomes make the c-PNG a suitable candidate for use in electronic skin applications and wearable devices.

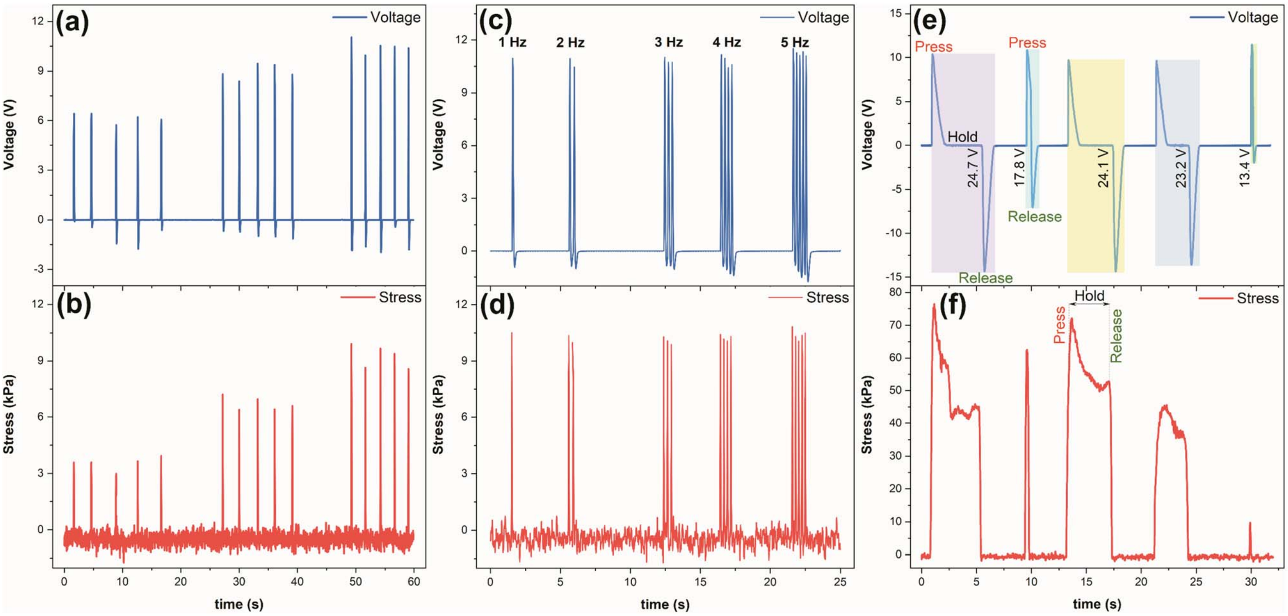

Fig. 5 Results of the simultaneous recording of the open-circuit voltage and the applied stress under finger tapping. Effect of the applied stress (a) amplitude, (c) frequency and (e) duration on the open-circuit voltage. (b, d and f) The corresponding applied mechanical stress under finger tapping.

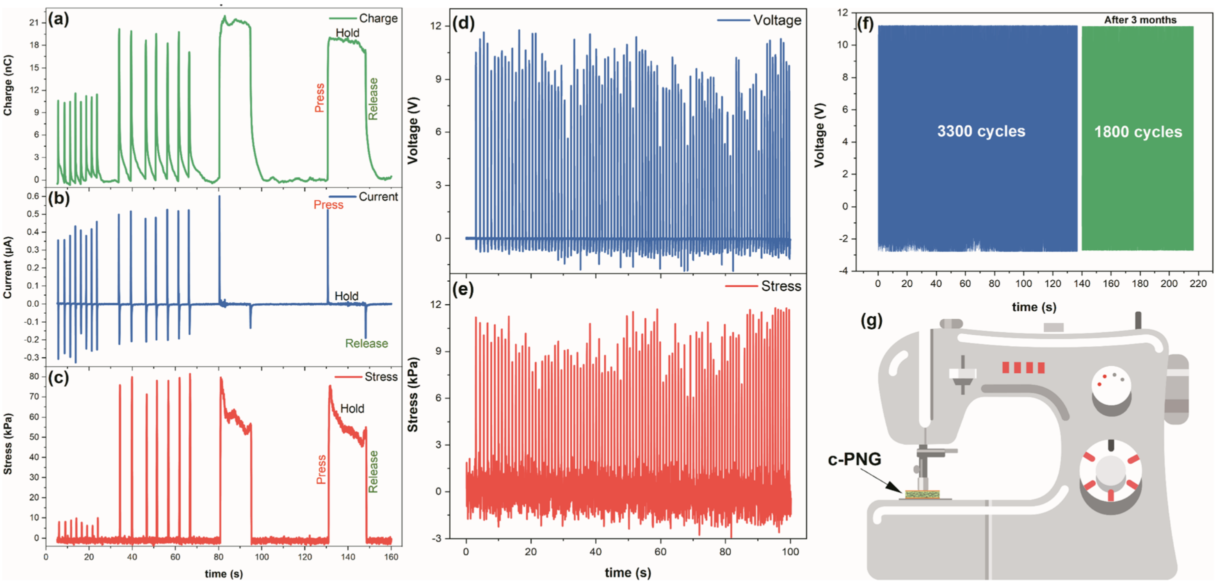

Fig. 6 Real-time recording of the (a) electrical charges and (b) current and (c) the corresponding mechanical stress under finger tapping using the flexible piezocomposite nanogenerator device. The test results of the reliability and durability of the fabricated c-PNG device. (d) Open-circuit voltage and (e) the corresponding applied stress under successive finger tapping. (f) Stability and durability of the open-circuit voltage after three months under sewing machine impartations, and (g) illustration of the open-circuit voltage stability testing of the c-PNG using sewing machine impartations.

By employing the same approach of the simultaneous recording of the mechanical and electrical outputs, the dependence of the electrical charges and current with the applied stress can be deduced, as presented in Fig. 6a–c. It is clearly shown that the values of the electrical charges and the current change are stress-dependent, and applying high mechanical stress induces high electrical charges and current values. For instance, by applying 9.8 kPa, electrical charge and current values of 11.55 nC and 0.42 μA, respectively, are obtained. The calculated charge density of about 48.4 μC cm^{-2} is higher than that obtained in our previous work in a piezoelectric nanogenerator based on BCZT spherical nanoparticles and a PLA matrix.[27] As observed in the effect of the pressing duration on the open-circuit voltage, the charge and current can be further improved by adding the hold sequence in the mechanical input. Accordingly, our pioneering concept based on simultaneously recording the mechanical input and electrical outputs can be helpful to easily tune energy harvesting performances.

The voltage-stability testing of the fabricated piezocomposite nanogenerator was performed under gentle finger tapping (10 kPa) at a frequency of 1 Hz by measuring simultaneously both voltage and mechanical stress, as illustrated in Fig. 6d and e. It is observed that the output voltage is mechanical stress-dependent, and since it is difficult to maintain constant stress under finger tapping for a prolonged time, we used a sewing machine as a constant stress source (see Fig. 6f and g), as reported in our previous work.[27] After 3300 cycles, at a frequency of 23 Hz, constant voltage values were observed without any performance degradation or mechanical damage. Besides this, the durability of the output performance, which is by far the biggest downside of piezoelectric nanogenerators, was evaluated after 3 months of aging under 1800 tapping cycles using a sewing machine at a frequency of 23 Hz (Fig. 6f). A slight drop in the output voltage (<0.04 V) was detected without any mechanical damage of the piezoelectric nanogenerator during the tests. These outcomes prove the excellent performance stability of our mechanical energy harvester even after three months of aging.

3.3. Self-poling mechanism in the c-PNG

Self-polarisation has already been reported to be an amazing technique by which to eliminate the complexity of the traditional electrical poling process for piezoelectric and ferroelectric materials-based energy harvesting devices.[25,67] Similar to self-poled PVDF-based PNGs, the self-poling aspects in PLA results from some degree of molecular alignment of the PLA chains along the length of the HZTO-nw and BCZT-mp.[25] In other words, the PLA molecules are self-polarised in a favourable direction *via* the dual effect of stress and surface charge induced polarisation without the application of an external electric field. It has been reported that the electroactive β-phase of PLA has flexible molecular chains containing C═O dipoles, where the crystal structure is characterised by a helical structure and the shear piezoelectricity at the molecular level originates from the dipole that accompanies the asymmetric carbon.[68] The amount of the β-phase in PLA could be increased by embedding piezoelectric fillers into the PLA matrix, thus enhancing the piezoelectric properties. In our case, the presence of the oppositely charged polar surfaces on HZTO-nw and BCZT-mp aggressively interact with the different C═O dipoles of PLA, resulting in the developing of negative and positive charge densities over the nanocomposite surface, promoting the formation of a piezoelectric polar β-phase through surface charge induced polarisation. Besides this, the applied mechanical strain induces a potential in the HZTO-nw and BCZT-mp which additionally aligns the C═O dipoles in the direction of the applied force through stress induced polarisation. Accordingly, the use of the PLA biopolymer eliminates the complexity of the traditional electrical poling process in piezoelectric energy harvesters.

3.4. Some applications of the c-PNG

In biomechanical energy harvesting, an effective piezoelectric nanogenerator is regarded to generate electrical energy from various motions (compressive stress, bending, stretching, folding, *etc.*).[25,69,70] To shed more light on this concept, the ability of the c-PNG to generate electricity from bending motions was investigated. As presented in Fig. 7a, our energy harvesting system can operate effectively under bending/unbending motions under a reverse connection mode, and can generate a maximum voltage of around 2.5 V, with a peak-to-peak voltage of >6.5 V. The results of the voltage-stability testing under finger bending/unbending are shown in Fig. S8 (ESI)†.

Fig. 7b illustrates the load voltage and instantaneous power of the c-PNG device recorded as a function of various external resistive loads (R_L) from 1 kΩ to 50 MΩ, as shown in the schematic circuit diagram in the inset of Fig. 7b. Increasing the load resistance gradually increases the output voltage to the open-circuit value. This behaviour is characteristic of piezoelectric nanogenerators.[71,72] The instantaneous power calculated by $P_{\max} = V^2/R_L$ increases with increasing resistance up to a maximum value ($P_{\max}$) of 17.5 μW under an external load of 4 MΩ and then decreases upon further increasing the resistance. The obtained $P_{\max}$ value is among the highest reported for piezoelectric nanogenerators at reasonably low load resistance.[3,19,27] The corresponding volumetric power density was calculated to be 9.2 mW cm^{-3}. This value is far higher than the values reported in the overwhelming majority of the previous reports on composite film based piezoelectric nanogenerators.[21,27,72–74] It was apprehended that the experimentally measured current (I, 0.6 μA) is lower than that estimated theoretically using the equation $I = \sqrt{P_{\max}/R_L}$ (2.1 μA). This discrepancy is generally due to the power consumption of internal resistance present in the measurement system.[25,75]

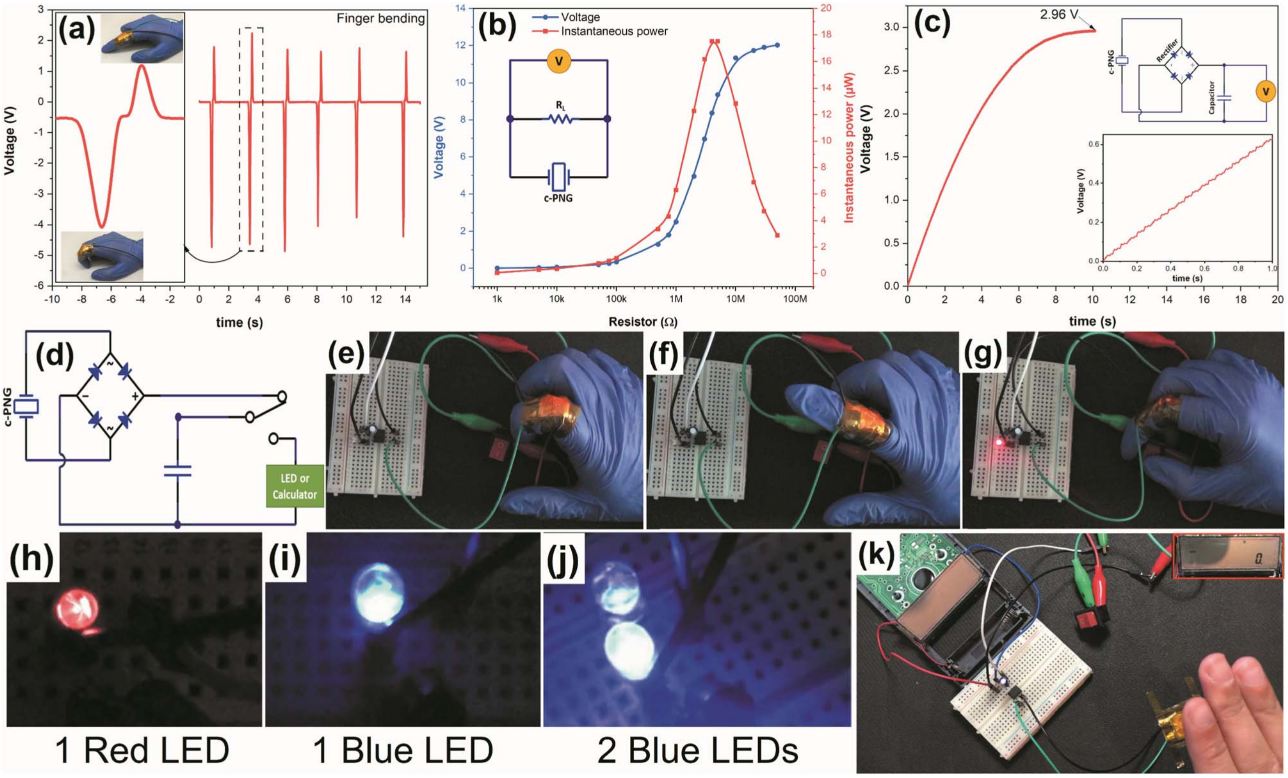

Fig. 7 The test results of the feasibility of the fabricated c-PNG device. (a) The generated open-circuit voltage of the c-PNG device when attached to the forefinger and stressed by successive biomechanical bending motions. (b) The measured voltage and calculated instantaneous output power under varied external resistance loads in the range from 1 kΩ to 50 MΩ (the inset shows the electrical circuit diagram used to measure the harvested output voltage). (c) The charging curve of a 1 μF-capacitor using the piezocomposite nanogenerator under sewing machine impartations (the inset shows the electrical circuit diagram used to harvest the electric energy from the c-PNG device (top) and an enlarged view of the charging curve (bottom)). (d) Schematic circuit diagram of the LEDs and calculator powering using the c-PNG. (e–g) Photographic images of the process of the red LED glowing under finger bending/unbending using the c-PNG. (h–j) Captured photographs showing various LEDs being lit up by the electric energy generated from the c-PNG device. (k) Captured photograph of a commercial calculator powered by the c-PNG under successive hand slapping impartations (the inset shows the calculator display turning on).

To check the feasibility of the c-PNG to be integrated as a powering device for small portable electronic applications and flexible high energy density capacitors, several tests were conducted. First, the c-PNG device was used to charge a 1 μF-capacitor under sewing machine impartations at a frequency of 23 Hz. The top inset of Fig. 7c shows the schematic circuit diagram used to track the accumulated voltage during the capacitor charging, which includes a full-wave bridge rectifier, 1 μF capacitor, and the piezoelectric nanogenerator. The bottom inset presents an enlarged view of the voltage–time curve recorded during the capacitor charging process. The c-PNG can charge the 1 μF capacitor up to 2.96 V in a very short time span of 10 s, which corresponds to $U_e = 1/2CV^2$, to a stored energy of 4.38 μJ and an equivalent energy density of 2.3 mJ cm^{-3}. Here U_e, C, and V refer to the stored electric density, capacitor capacity, and the generated voltage, respectively.

Besides the energy storage capability, we also demonstrated the realistic usefulness of the c-PNG with energy generating capability to drive different types of commercial electronics, such as light-emitting diodes (LEDs) and a calculator. Using the schematic circuit diagram in Fig. 7d, the power generated from the c-PNG under cyclic finger tapping or hand slapping impartations was stored in a 10 μF-capacitor, and then could turn on: one red LED under finger bending (Fig. 7e–g and Video S3 (ESI)),† one red LED under finger tapping (Fig. 7h and Video S4 (ESI)),† one blue LED and two blue LEDs (Fig. 7i and j and Video S5 (ESI)),† and a calculator (Fig. 7k and Video S6 (ESI))† after successive hand slapping impartations for five min. The results of these tests verify the c-PNG as a capable energy harvesting device for regular and irregular excitations present in our living or harsh environments and as a powering device for small portable electronics.

4. Conclusions

In this study, we reported a new conceptual strategy to design ceramic/polymer nanocomposites for mechanical energy harvesting applications, involving the embedding of HZTO nanowires and BCZT multipods in a PLA biopolymer. Through the simultaneous recording of the mechanical input (stress under finger tapping) and the electric outputs (open-circuit voltage, short-circuit current and electrical charges), we can easily tune the energy harvesting performance. The c-PNG device demonstrated an enhanced output voltage, current and volumetric power density of 11.5 V, 0.6 μA and 9.2 mW cm^{-3}, respectively, under cyclic finger imparting, alongside a high-pressure sensitivity of 0.86 V kPa^{-1} and fast response time of 45 ms at 1 Hz. Besides this, the c-PNG can generate a highly stable and durable output voltage, even after three months, proving its applicability to power commercial electronics (charging capacitors, glowing LEDs and powering a calculator). Multi-physics simulations using COMSOL Multiphysics indicate that the presence of BCZT-mp was crucial in enhancing the piezoelectric response of the c-PNG. Accordingly, the embedding of HZTO-nw (1D) and BCZT-mp (3D) in a PLA composite-based PNG paves the way for a new and effective strategy to design eco-friendly and flexible devices for powering small portable electronics and could be beneficial in enhancing mechanical energy harvesting properties.

Authors contribution

Zouhair Hanani: conceptualisation, formal analysis, investigation, data curation, methodology, writing – original draft. Ilyasse Izanzar: conceptualisation, investigation, data curation, methodology. Soukaina Merselmiz: conceptualisation, data curation, visualisation. M'barek Amjoud: supervision. Daoud Mezzane: supervision, funding acquisition. Jaafar Ghanbaja: resources, investigation. Ismael Saadoune: resources. Mohammed Lahcini: supervision, resources. Matjaž Spreitzer: Resources, funding acquisition, writing – review & editing, Validation. Damjan Vengust: investigation, data curation. Mimoun El Marssi: resources, project administration, funding acquisition. Igor A. Luk'yanchuk: project administration, validation, funding acquisition, writing – review & editing. Zdravko Kutnjak: project administration, resources, Validation, funding acquisition, writing – review & editing. Mohamed Gouné: supervision, project administration, funding acquisition.

Conflicts of interest

There are no conflicts to declare.

Acknowledgements

The authors gratefully acknowledge the generous financial support of the European Union Horizon 2020 Research and Innovation actions MSCA-RISE-ENGIMA (No. 778072) and MSCA-RISE-MELON (No. 872631). Z. K. and M. S. acknowledge the Slovenian Research Agency program P1-0125 and P2-0091, respectively.

References

1 Z. L. Wang and J. Song, *Science*, 2006, **312**, 242–246.

2 D. Hu, M. Yao, Y. Fan, C. Ma, M. Fan and M. Liu, *Nano Energy*, 2019, **55**, 288–304.

3 E. L. Tsege, G. H. Kim, V. Annapureddy, B. Kim, H. K. Kim and Y. H. Hwang, *RSC Adv.*, 2016, **6**, 81426–81435.

4 D. K. Khatua and S.-J. Kim, *J. Mater. Chem. C*, 2022, **10**, 2905–2924.

5 P. Zhu, B. Zhang, H. Wang, Y. Wu, H. Cao, L. He, C. Li, X. Luo, X. Li and Y. Mao, *Nano Res.*, 2022, **15**, 7460–7467.

6 Y. Tang, H. Zhou, X. Sun, N. Diao, J. Wang, B. Zhang, C. Qin, E. Liang and Y. Mao, *Adv. Funct. Mater.*, 2020, **30**, 1907893.

7 S. Xiang, D. Liu, C. Jiang, W. Zhou, D. Ling, W. Zheng, X. Sun, X. Li, Y. Mao and C. Shan, *Adv. Funct. Mater.*, 2021, **31**, 2100940.

8 X. Li, P. Zhu, S. Zhang, X. Wang, X. Luo, Z. Leng, H. Zhou, Z. Pan and Y. Mao, *ACS Nano*, 2022, **16**, 5909–5919.

9 M. Pan, C. Yuan, X. Liang, J. Zou, Y. Zhang and C. Bowen, *iScience*, 2020, **23**, 101682.

10 M. A. Parvez Mahmud, N. Huda, S. H. Farjana, M. Asadnia and C. Lang, *Adv. Energy Mater.*, 2018, **8**, 1–25.

11 Y. Zhang, M. Wu, Q. Zhu, F. Wang, H. Su, H. Li, C. Diao, H. Zheng, Y. Wu and Z. L. Wang, *Adv. Funct. Mater.*, 2019, **29**, 1904259.

12 Z. Zhou, Z. Zhang, Q. Zhang, H. Yang, Y. Zhu, Y. Wang and L. Chen, *ACS Appl. Mater. Interfaces*, 2020, **12**, 1567–1576.

13 M. Yao, Y. Pu, L. Zhang and M. Chen, *Mater. Lett.*, 2016, **174**, 110–113.

14 J. Koruza, A. J. Bell, T. Frömling, K. G. Webber, K. Wang and J. Rödel, *J. Mater.*, 2018, **4**, 13–26.

15 E. Cross, *Nature*, 2004, **432**, 24–25.

16 S. Merselmiz, Z. Hanani, D. Mezzane, A. G. Razumnaya, M. Amjoud, L. Hajji, S. Terenchuk, B. Rožič, I. A. Lukyanchuk and Z. Kutnjak, *RSC Adv.*, 2021, **11**, 9459–9468.

17 S. Merselmiz, Z. Hanani, U. Prah, D. Mezzane, L. Hajji, Z. Abkhar, M. Spreitzer, D. Vengust, H. Uršič, D. Fabijan, A. G. Razumnaya, O. Shapovalova, I. A. Lukyanchuk and Z. Kutnjak, *Phys. Chem. Chem. Phys.*, 2022, **24**, 6026–6036.

18 Z. H. Lin, Y. Yang, J. M. Wu, Y. Liu, F. Zhang and Z. L. Wang, *J. Phys. Chem. Lett.*, 2012, **3**, 3599–3604.

19 K. S. Chary, V. Kumar, C. D. Prasad and H. S. Panda, *J. Aust. Ceram. Soc.*, 2020, **56**, 1107–1117.

20 K.-I. Park, C. K. Jeong, N. K. Kim and K. J. Lee, *Nano Converg.*, 2016, **3**, 12.

21 D. J. Shin, J. H. Ji, J. Kim, G. H. Jo, S. J. Jeong and J. H. Koh, *J. Alloys Compd.*, 2019, **802**, 562–572.

22 J. H. Jung, C. Y. Chen, B. K. Yun, N. Lee, Y. Zhou, W. Jo, L. J. Chou and Z. L. Wang, *Nanotechnology*, 2012, **23**, 375401.

23 K. Il Park, J. H. Son, G. T. Hwang, C. K. Jeong, J. Ryu, M. Koo, I. Choi, S. H. Lee, M. Byun, Z. L. Wang and K. J. Lee, *Adv. Mater.*, 2014, **26**, 2514–2520.

24 K. Ibtehaj, M. H. Hj Jumali and S. Al-Bati, *Polymer*, 2020, **208**, 122956.

25 S. K. Karan, R. Bera, S. Paria, A. K. Das, S. Maiti, A. Maitra and B. B. Khatua, *Adv. Energy Mater.*, 2016, **6**, 1601016.

26 S. K. Karan, S. Maiti, J. H. Lee, Y. K. Mishra, B. B. Khatua and J. K. Kim, *Adv. Funct. Mater.*, 2020, **30**, 2004446.

27 Z. Hanani, I. Izanzar, M. Amjoud, D. Mezzane, M. Lahcini, H. Uršič, U. Prah, I. Saadoune, M. El Marssi, I. A. Luk'yanchuk, Z. Kutnjak and M. Gouné, *Nano Energy*, 2021, **81**, 105661.

28 Z. Zhou, C. C. Bowland, M. H. Malakooti, H. Tang and H. A. Sodano, *Nanoscale*, 2016, **8**, 5098–5105.

29 C. K. Jeong, C. Baek, A. I. Kingon, K. Il Park and S. H. Kim, *Small*, 2018, **14**, 1704022.

30 Z. Hanani, I. Izanzar, S. Merselmiz, T. El Assimi, D. Mezzane, M. Amjoud, H. Uršič, U. Prah, J. Ghanbaja, I. Saadoune, M. Lahcini, M. Spreitzer, D. Vengust, M. El Marssi, Z. Kutnjak, I. A. Lukyanchuk and M. Gouné, *Sustainable Energy Fuels*, 2022, **6**, 1983–1991.

31 G. Jian, Y. Jiao, Q. Meng, Y. Guo, F. Wang, J. Zhang, C. Wang, K. S. Moon and C. P. Wong, *Nano Energy*, 2021, **82**, 105778.

32 G. Jian, Y. Jiao, Q. Meng, H. Shao, F. Wang and Z. Wei, *Adv. Mater. Interfaces*, 2020, **7**, 2000484.

33 D. H. Kim, B. Dudem and J. S. Yu, *ACS Sustainable Chem. Eng.*, 2018, **6**, 8525–8535.

34 Z. Hanani, D. mezzane, M. Amjoud, M. Lachini, M. Spreitzer, D. Vengust, A. Jamali, M. El Marssi, Z. Kutnjak and M. Gouné, *J. Mater. Chem. C*, 2022, **10**, 10823–10831.

35 Z. Hanani, E. H. Ablouh, M. Barek Amjoud, D. Mezzane, S. Fourcade and M. Gouné, *Ceram. Int.*, 2018, **44**, 10997–11000.

36 Z. Hanani, E. H. Ablouh, S. Merselmiz, J. Ghanbaja, M. Amjoud, D. Mezzane, A. Alimoussa, M. Lahcini, M. Spreitzer, D. Vengust, M. El Marssi, I. A. Lukyanchuk, Z. Kutnjak and M. Gouné, *CrystEngComm*, 2021, **23**, 5249–5256.

37 Z. Hanani, S. Merselmiz, M. Amjoud, D. Mezzane, M. Lahcini, J. Ghanbaja, M. Spreitzer, D. Vengust, M. El Marssi, I. A. Lukyanchuk, Z. Kutnjak, B. Rožič and M. Gouné, *J. Mater.*, 2022, **8**, 873–881.

38 Y. Fan, X. Huang, G. Wang and P. Jiang, *J. Phys. Chem. C*, 2015, **119**, 27330–27339.

39 P. Hu, S. Gao, Y. Zhang, L. Zhang and C. Wang, *Compos. Sci. Technol.*, 2018, **156**, 109–116.

40 T. El Assimi, R. Blažic, A. El Kadib, M. Raihane, R. Beniazza, G. A. Luinstra, E. Vidović and M. Lahcini, *Carbohydr. Polym.*, 2019, **220**, 95–102.

41 H. Zhang, J. Huang, L. Yang, R. Chen, W. Zou, X. Lin and J. Qu, *RSC Adv.*, 2015, **5**, 4639–4647.

42 T. El Assimi, R. Blažic, E. Vidović, M. Raihane, A. El Meziane, M. H. V. Baouab, M. Khouloud, R. Beniazza, H. Kricheldorf and M. Lahcini, *Prog. Org. Coat.*, 2021, **156**, 106255.

43 T. Wu, Y. Song, Z. Shi, D. Liu, S. Chen, C. Xiong and Q. Yang, *Nano Energy*, 2021, **80**, 105541.

44 H. S. Kim, D. W. Lee, D. H. Kim, D. S. Kong, J. Choi, M. Lee, G. Murillo and J. H. Jung, *Nanomaterials*, 2018, **8**, 777.

45 X. Meng, Z. Zhang, D. Lin, W. Liu, S. Zhou, S. Ge, Y. Su, C. Peng and L. Zhang, *J. Adv. Ceram.*, 2021, **10**, 991–1000.

46 L. Ye, L. Chen, J. Yu, S. Tu, B. Yan, Y. Zhao, X. Bai, Y. Gu and S. Chen, *J. Mater. Sci. Mater. Electron.*, 2021, **32**, 3966–3978.

47 G. Zhang, Q. Liao, Z. Zhang, Q. Liang, Y. Zhao, X. Zheng and Y. Zhang, *Adv. Sci.*, 2015, **3**, 1500257.

48 C. Baek, J. H. Yun, J. E. Wang, C. K. Jeong, K. J. Lee, K. Il Park and D. K. Kim, *Nanoscale*, 2016, **8**, 17632–17638.

49 T. Kamilya, P. K. Sarkar and S. Acharya, *ACS Omega*, 2019, **4**, 17684–17690.

50 Z. Wang, W. Liu, J. Hu, W. He, H. Yang, C. Ling, Y. Xi, X. Wang, A. Liu and C. Hu, *Nano Energy*, 2020, **69**, 104452.

51 M. F. Lin, J. Xiong, J. Wang, K. Parida and P. S. Lee, *Nano Energy*, 2018, **44**, 248–255.

52 K. Parida, V. Bhavanasi, V. Kumar, R. Bendi and P. S. Lee, *Nano Res.*, 2017, **10**, 3557–3570.

53 W. Guo, C. Tan, K. Shi, J. Li, X. X. Wang, B. Sun, X. Huang, Y. Z. Long and P. Jiang, *Nanoscale*, 2018, **10**, 17751–17760.

54 X. Gao, M. Zheng, X. Yan, J. Fu, M. Zhu and Y. Hou, *J. Mater. Chem. C*, 2019, **7**, 961–967.

55 L. Natta, V. M. Mastronardi, F. Guido, L. Algieri, S. Puce, F. Pisano, F. Rizzi, R. Pulli, A. Qualtieri and M. De Vittorio, *Sci. Rep.*, 2019, **9**, 8392.

56 A. S. Dahiya, F. Morini, S. Boubenia, K. Nadaud, D. Alquier and G. Poulin-Vittrant, *Adv. Mater. Technol.*, 2018, **3**, 1700249.

57 P. Bai, G. Zhu, Q. Jing, J. Yang, J. Chen, Y. Su, J. Ma, G. Zhang and Z. L. Wang, *Adv. Funct. Mater.*, 2014, **24**, 5807–5813.

58 Q. L. Zhao, G. P. He, J. J. Di, W. L. Song, Z. L. Hou, P. P. Tan, D. W. Wang and M. S. Cao, *ACS Appl. Mater. Interfaces*, 2017, **9**, 24696–24703.

59 D. Yu, Z. Zheng, J. Liu, H. Xiao, G. Huangfu and Y. Guo, *Nano-Micro Lett.*, 2021, **13**, 117.

60 G. Zhao, Y. Zhang, N. Shi, Z. Liu, X. Zhang, M. Wu, C. Pan, H. Liu, L. Li and Z. L. Wang, *Nano Energy*, 2019, **59**, 302–310.

61 H. Liu, X. Lin, S. Zhang, Y. Huan, S. Huang and X. Cheng, *J. Mater. Chem. A*, 2020, **8**, 19631–19640.

62 Y. Zhou, J. He, H. Wang, K. Qi, N. Nan, X. You, W. Shao, L. Wang, B. Ding and S. Cui, *Sci. Rep.*, 2017, **7**, 12949.

63 D. Y. Park, D. J. Joe, D. H. Kim, H. Park, J. H. Han, C. K. Jeong, H. Park, J. G. Park, B. Joung and K. J. Lee, *Adv. Mater.*, 2017, **29**, 1702308.

64 J. Luo, L. Zhang, T. Wu, H. Song and C. Tang, *Extrem. Mech. Lett.*, 2021, 101279.

65 W. Choi, J. Lee, Y. Kyoung Yoo, S. Kang, J. Kim and J. Hoon Lee, *Appl. Phys. Lett.*, 2014, **104**, 123701.

66 J. C. Yang, J. O. Kim, J. Oh, S. Y. Kwon, J. Y. Sim, D. W. Kim, H. B. Choi and S. Park, *ACS Appl. Mater. Interfaces*, 2019, **11**, 19472–19480.

67 B. Bagchi, N. A. Hoque, N. Janowicz, S. Das and M. K. Tiwari, *Nano Energy*, 2020, **78**, 105339.

68 H. J. Oh, D. K. Kim, Y. C. Choi, S. J. Lim, J. B. Jeong, J. H. Ko, W. G. Hahm, S. W. Kim, Y. Lee, H. Kim and B. J. Yeang, *Sci. Rep.*, 2020, **10**, 16339.

69 S. K. Si, S. K. Karan, S. Paria, A. Maitra, A. K. Das, R. Bera, A. Bera, L. Halder and B. B. Khatua, *Mater. Chem. Phys.*, 2018, **213**, 525–537.

70 X. Niu, W. Jia, S. Qian, J. Zhu, J. Zhang, X. Hou, J. Mu, W. Geng, J. Cho, J. He and X. Chou, *ACS Sustainable Chem. Eng.*, 2019, **7**, 979–985.

71 K. Il Park, S. Bin Bae, S. H. Yang, H. I. Lee, K. Lee and S. J. Lee, *Nanoscale*, 2014, **6**, 8962–8968.

72 N. A. Hoque, P. Thakur, P. Biswas, M. M. Saikh, S. Roy, B. Bagchi, S. Das and P. P. Ray, *J. Mater. Chem. A*, 2018, **6**, 13848–13858.

73 R. Zhu, J. Jiang, Z. Wang, Z. Cheng and H. Kimura, *RSC Adv.*, 2016, **6**, 66451–66456.

74 K. Il Park, S. Xu, Y. Liu, G. T. Hwang, S. J. L. Kang, Z. L. Wang and K. J. Lee, *Nano Lett.*, 2010, **10**, 4939–4943.

75 M. M. Alam and D. Mandal, *ACS Appl. Mater. Interfaces*, 2016, **8**, 1555–1558.